ARTICLE

Synthesis, Characterization and Photoinduced CO Release by Manganse(I) Complexes

Received 00th January 20xx,
Accepted 00th January 20xx

DOI: 10.1039/x0xx00000x

André L. Amorim[a,†], Ana Guerreiro[b,†], Vinícius A. Glitz[a], Daniel F. Coimbra[a], Adailton J. Bortoluzzi[a], Giovanni F. Caramori[a], Antonio L. Braga[a], Ademir Neves[a], Gonçalo J. L. Bernardes[b,c,*] and Rosely A. Peralta[a,*]

Herein, we report the CO-release activity of three new photoCORMs, two with nonbonding pyridine moieties and one with a benzyl group. The compounds [MnBr(CO)$_3$(bpa-κ^2)] (**2**, where bpa = *N*-benzyl(2-pyridylmethyl)amine); [MnBr(CO)$_3$(pmpea-κ^2)] (**3**, where pmpea = *N*-(2-pyridylmethyl)-*N'*-(2-pyridylethyl)amine) and [MnBr(CO)$_3$(bpea-κ^2)] (**4**, where bpea = *N*-bis(2-pyridylethyl)amine) were synthesized and characterized by common spectroscopic techniques (UV-Vis, IR). Density functional theory studies were also performed to provide new insights into the M–C bond and to assume the orbitals involved in the absorption transitions. Their CO-release activities were measured both in organic and in physiological media and compared to that of a previously published compound [Mn(CO)$_3$(dpa-κ^3)]Br (**1**, where dpa = *N*-bis(2-pyridylmethyl)amine). An increase in the number of members of the chelate from five to six, influenced the release of CO, affecting both the binding mode of the ligand and the CO-release process and affecting their potential use as potentials CO release carriers as therapeutic agents.

Introduction

The discovery of signaling molecules that can control biological functions has opened many possibilities in the fields of medicinal and bioinorganic chemistry. Although nitric oxide is among the most prominent signaling molecules,[1] in recent years carbon monoxide has also been recognized as a signaling molecule in biological media.[2–4] The cytotoxic effects are widely known,[5] but carbon monoxide can also act in vital physiological processes, such as the regulation of ion-channels, and as a neurotransmitter, inhibitor of platelet coagulation and suppressor of acute hypertension.[6–8]

The controlled delivery of exogenous carbon monoxide has been used to protect against lung injury in vivo, as an anti-inflammatory agent, to trigger cell apoptosis and to promote antioxidant activity.[9–12] All of these properties support the use of CO as a versatile agent in medicinal chemistry. However, the high affinity of carbon monoxide for hemoglobin poses both a problem and a risk in relation to its use in high concentrations. Therefore, the development of new compounds that avoid the drawbacks of exogenously applied CO[13] and that have the capacity to deliver carbon monoxide in a controlled manner is highly desirable.[14] In this regard, low-valence metal carbonyl compounds can serve as favourable vehicles to transport carbon monoxide, given their interesting spectroscopic properties and the wide array of ligand modifications that can influence the CO release activity. The metal centres most commonly studied as possible CORMs candidates include iron, rhenium, molybdenum and manganese.[15–18]

There are several ways to promote the release of CO from these molecules and photoexcitation is one of the preferred methods. The first photoCORMs synthesized only showed activity in the UV light range, which represents a drawback in biological studies due to the potentially mutagenic nature of UV light.[19] To overcome this difficulty, some research groups have been using ligands that shift either the carbon monoxide MLCT or the intraligand bands towards lower energy to facilitate CO release at higher wavelengths.[20,21] In this context, some advances using conjugated polypyridyls and conjugated imine groups and softer ligands have been made.[22,23]

Nevertheless, the literature still lacks information on modifications around the metal center, in which nonbonding moieties are used in the ligand framework, and their influence on CO-release activity.

Herein, we report three new manganese photoCORMs (Fig. 1), one with a noncoordinating benzyl moiety (**2**) and two that have a nonbonding pyridine in the coordination sphere (**3**, **4**).

[a] Departamento de Química, Universidade Federal de Santa Catarina, Florianópolis, Santa Catarina, Brazil;Post code: 88040-900; Tel +55(48)3721-3627; E-mail: rosely.peralta@ufsc.br
[b] Instituto de Medicina Molecular, Faculdade de Medicina, Universidade de Lisboa, Avenida Professor Egas Moniz, P.O. Box: 1649-028, Lisboa, Portugal; Tel: +351-217-999-567; E-mail: gbernardes@medicina.ulisboa.pt
[c] Departament of Chemistry, University of Cambridge, Cambridge, United Kingdom, Lensfied Road, P.O. Box: CB2 1EW, E-mail: gb453@cam.ac.uk; Homepage: www.gbernardeslab.com

† These authors contributed equally to this work.

Electronic Supplementary Information (ESI) available: [details of any supplementary information available should be included here]. See DOI: 10.1039/x0xx00000x

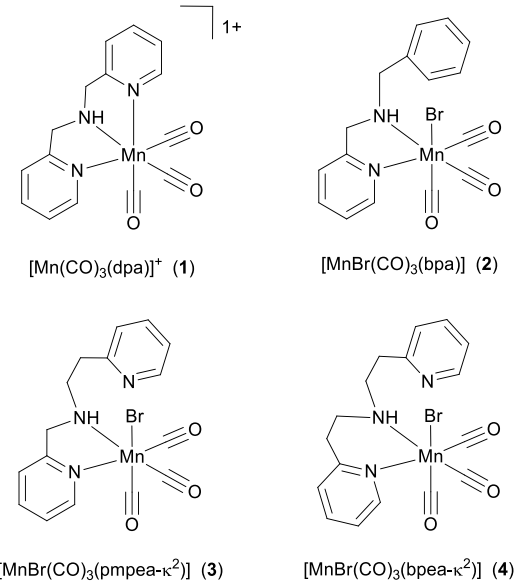

Fig. 1 Representation of the structures of the manganese carbonyls used in this study.

Because photo-release studies were conducted on a custom-made LED apparatus and the CO release activity is highly dependent on the way incident light is focused, the compound $[Mn(CO)_3(dpa\text{-}\kappa^3)]Br$ (**1**, where dpa = *N*-bis(2-pyridylmethyl)amine), previously reported by Gonzalez,[24] was revisited in the light of new insights and its photo-release capabilities were compared to those of the synthesized metal carbonyls.

The synthesis, characterization and evaluation of the biological activity of three new carbonyl compounds: [MnBr(CO)3(bpa-κ²)] (**2**, where bpa = *N*-benzyl(2-pyridylmethyl)amine) and $[MnBr(CO)_3(pmpea\text{-}\kappa^2)]$ (**3**, where pmpea = *N*-(2-pyridylmethyl)-*N*-amine) and $[MnBr(CO)_3(bpea\text{-}\kappa^2)]$ (**4**, where bpea = *N*-bis(2-pyridylethyl)amine) are also reported herein. The compounds were characterized by using standard techniques, such as IR, UV-Vis and X-ray spectroscopy and mass spectrometry. The stability and the CO release activity were monitored by using well-known methods previously described in the literature,[9] and the modifications were accompanied on electronic absorption spectra at different wavelengths.

Experimental Section

General procedures

Ligands dpa, bpa, pmpea and bpea were synthesized analogously to previously published procedures[25–28] and their schematic representations are shown in Fig. 1. The reactants used for the synthesis of the ligands and complexes were purchased from Merck. The reagents benzaldehyde, 2-aminomethylpyridine, 2-aminoethylpyridine, pyridylcarboxyaldehyde and 2-vinylpyridine were distilled under reduced pressured and stored in an appropriate flask under argon at low temperature before use.

Synthesis of the organometallic compounds

The synthesis of compounds **1**–**4** was performed under an inert atmosphere with a conventional Schlenk apparatus and all solvents used in the reactions were purified prior to use by standard procedures. Previously published compound $[Mn(CO)_3(dpa\text{-}\kappa^3)]Br$ (**1**) was synthesized according to the literature[24] and used for comparison. For the preparation of $[MnBr(CO)_3(bpa\text{-}\kappa^2)]$ (**2**), $[MnBr(CO)_3(pmpea\text{-}\kappa^2)]$ (**3**) and $[MnBr(CO)_3(bpea\text{-}\kappa^2)]$ (4), a solution containing 0.25 mmol of the ligand (bpa, pmpea or bpea) in 10 mL of diethyl ether was degassed applying two freeze-pump-thaw cycles. The manganese precursor $[MnBr(CO)_5]$ (0.25 mmol) was added to a frozen solution of the ligand and the solution was thawed once more. The resulting solution stirred until the mixture reached room temperature. It was then heat to reflux under an inert atmosphere and dim light conditions for 12 h. The solvent was removed from the resulting solution under reduced pressure, providing a yellow solid. Crystals suitable for X-ray analysis were obtained by slow diffusion of hexane in a dichloromethane solution.

$[Mn(CO)_3(dpa\text{-}\kappa^3)]Br$ (**1**): pale yellow solid, yield: 74 mg; 418.12 g mol^{-1}, 71%. Selected IR frequencies (ATR, cm^{-1}): 2025 (s, ν_{CO}), 1935 (s, ν_{CO}), 1910 (s, ν_{CO}), 1605-1435 (w, ν_{ar}), 760 (m, δ_{ar}), 630 (m, δ_{ar}). Selected electronic absorption wavelengths (CH_2Cl_2, λ_{max} in nm) and their respective ε values (L mol^{-1} cm^{-1}): 350 (2407), 300 (4250), 268 (4700), 244 (8019). MS (CH_3CN, ESI, *m/z*): 338 $[Mn(CO)_3(dpa\text{-}\kappa^2)]^+$. Elemental analysis for ($C_{15}H_{13}N_3O_3MnBr + H_2O$) (calculated in parenthesis): C, 42.52 (41.31); H, 3.37 (3.47); N, 9.70 (9.63).

$[MnBr(CO)_3(bpa\text{-}\kappa^2)]$ (**2**): pale yellow solid, yield: 78 mg; 416.15 g mol^{-1}, 75%. Selected IR frequencies (ATR, cm^{-1}): 2019 (s, ν_{CO}), 1914 (s, ν_{CO}), 1611-1437 (w, ν_{ar}), 764 (m, δ_{ar}), 627 (m, δ_{ar}). Selected electronic absorption wavelengths (CH_2Cl_2, λ_{max} in nm) and their respective ε values (L mol^{-1} cm^{-1}): 380 (1423), 322 (1840). Elemental analysis for ($C_{16}H_{14}N_2O_3MnBr + H_2O$) (calculated in parenthesis): C, 43.65 (44.16); H, 3.46 (3.71); N, 6.34 (6.44).

$[MnBr(CO)_3(pmpea\text{-}\kappa^2)]Br$ (**3**): yellow solid, yield: 68 mg; 432.15 g mol^{-1}, 63%. Selected IR frequencies (ATR, cm^{-1}): 2020 (s, ν_{CO}), 1910 (s, ν_{CO}), 1605-1385 (w, ν_{ar}), 770 (m, δ_{ar}), 630 (m, δ_{ar}). Selected electronic absorption wavelengths (CH_2Cl_2, λ_{max} in nm) and their respective ε values (L mol^{-1} cm^{-1}): 355 (2078), 288 (4525), 253 (6927). MS (CH_3CN, ESI, *m/z*): 352 $[Mn(CO)_3(pmpea\text{-}\kappa^3)]^+$. Elemental analysis for ($C_{16}H_{15}N_3O_3MnBr$) (calculated in parenthesis): C, 43.87 (44.47); H, 3.37 (3.50); N, 9.62 (9.72).

$[Mn(CO)_3(bpea\text{-}\kappa^2)]Br$ (**4**): yellow solid, yield: 64 mg; 446.18 g mol^{-1}, 58%. Selected IR frequencies (ATR, cm^{-1}): 2020 (s, ν_{CO}), 1905 (s, ν_{CO}), 1605-1380 (w, ν_{ar}), 760 (m, δ_{ar}), 630 (m, δ_{ar}). Selected electronic absorption wavelengths (CH_2Cl_2, λ_{max} in nm)

and their respective ε values (L mol^{-1} cm^{-1}): 370 (1903), 298 (4561), 269 (7908). MS (CH_3CN, ESI, *m/z*): 366 [$Mn(CO)_3$(bpea-κ^3)]$^+$. Elemental analysis for ($C_{17}H_{17}N_3O_3MnBr$) (calculated in parenthesis): C, 45.15 (45.76); H, 3.76 (3.84); N, 9.28 (9.42).

Physical Measurements

IR spectra were obtained with a PerkinElmer Spectrum 100 FT-IR spectrophotometer with an ATR unit. Electrospray-ionization-mass spectrometry (ESI-MS) was carried on an Amazon-Ion Trap mass spectrometer in acetonitrile with an approximate concentration of 500 ppb. Electronic absorption spectra were obtained on a Varian Cary 50 UV-Vis spectrophotometer in quartz cuvettes of 1 cm path length. NMR spectroscopy was carried out with a Bruker Ascend 400 Varian FT-NMR 400 MHz setup using $CDCl_3$ as the solvent, at 25 °C. Chemical shifts were referenced to tetramethylsilane (TMS, δ = 0.00 ppm).

Single-Crystal X-ray Structure Determinations

Crystallographic analysis of compounds **1**, **3**, and **4** was carried out with a Bruker APEX II DUO diffractometer wit graphite-monochromated Mo-Kα radiation (λ = 0.071069 nm) at 200(2). Images were recorded by using the φ and ω scan method.[29] All intensities were corrected for Lorentz polarization effects and for absorption. The structures were solved by direct methods and refined by the full matrix least-squares methods using the SHELX program.[30] H atoms attached to C atoms were placed at their idealized positions, with C–H distances and U_{iso} values takes from the default settings of the refinement program. Hydrogen atoms of the amine groups were found on a Fourier difference map and treated as free atoms. ORTEP plots were drawn with the PLATON program.[31] Full crystallographic tables (including structure factors) for complexes 1, 3 and 4 have been deposited with the Cambridge Crystallographic Data Centre under supplementary publication numbers CCDC 1824854-1824856. These data can be obtained free of charge from the Cambridge Crystallographic Data Centre at www.ccdc.cam.ac.uk.

Computational Methods

Initially geometries for all compounds were obtained by using DFT[32,33] with the BP86[34] exchange correlation functional and Grimme's D3BJ dispersion correction[35] along with the Ahlrich basis sets[36–38] as implemented in the Orca package, version 3.0.2.[39] Structures were confirmed as minima by the absence of imaginary eigenvalues in the generalized Hessian matrix.

Kohn-Sham energy decomposition analysis (GKS-EDA) implemented in GAMESS-US 2012,[40] and the same protocols described for the geometry optimizations. The Boys and Bernardi approach[41] was used to correct for basis set superposition errors. In all cases a CO ligand was considered as one (neutral) fragment whereas the remainder of the molecule was the second fragment without residual charges. The GKS-EDA scheme decomposes the instantaneous interaction energy (ΔE_{int}) into the sum of six physical meaningful terms: electrostatic (ΔE_{elstat}), exchange (ΔE_{exch}), repulsion (ΔE_{rep}), polarization (ΔE_{pol}), dispersion (ΔE_{disp}) and correlation (ΔE_{corr}).

Absorption spectra of all compounds were obtained by using TD-DFT[42] and the same protocol described above, but with the B3LYP functional[43, 44] and the SMD solvation model.[45]

Cell culture

Two different cell lines were used for the in vitro studies, namely, HepG2 (a human hepatoma cell line) and HeLa cells (derived from cervical cancer cells). The cells were maintained in a humidified incubator at 37 °C in 5% CO_2 and grown in 1x Dulbecco's modified Eagle medium (D-MEM) with sodium pyruvate and without L-glutamine (Invitrogen, Life Technologies) supplemented with 10% heat-inactivated fetal bovine serum (FBS) (Gibco, Life Technologies), 1x MEM NEAA (Gibco, Life Technologies), 1X GlutaMAX (Gibco, Life technologies), 200 units mL^{-1} penicillin and 200 μg mL^{-1} streptomycin (Gibco, Life Technologies) and 10 mmol L^{-1} HEPES (Gibco, Life Technologies).

Cell viability assay

A total of 10^4 cells per well were seeded in 96-well plates and treated with either **1**–**4**, 24 h after the seeding, to allow the cells to stabilize. The cells were incubated with 1, 5, 10, 25, 50, 100 and 150 μmol L^{-1} of the carbonyl compounds for 24 h. After this incubation period, the culture medium was removed and the cells were incubated with CellTiter-Blue (Promega) for 90 min at 37 °C. The cell viability was evaluated by measuring the emission intensity in relative fluorescent units (RFUs) with an Infine M200 plate reader. After the reading, the cells were re-incubated with the complexes for an additional period of 24 h, giving a total incubation time of 48 h. The cell viability assay was performed as mentioned above for 24 h time point.

CO release in aqueous solution

The CO release profiles for compounds were determined in aqueous solution by COP-1 fluorescence,[46] at different time points (0, 10, 20, 30, 40, 50, 60, 70, 80 and 90 min). The COP-1 fluorescence was measured in the absence (negative control) and presence of 150 μmol L^{-1} of **1**-**4** using an Infinite M200 plate reader. The compounds were mixed with a 1 μmol L^{-1} solution of COP-1 (in PBS pH 7.4) previously prepared from a 5 μmol L^{-1} stock solution of COP-1 in DMSO. The COP-1 was synthesized according to a procedure described in the literature.[46] The measurements were taken in the range 490–610 nm.

CO release in cells measured by confocal microscopy

A total of 30^4 HeLa cells per well were seeded 24 h prior to the experiment in an 8-chambered Ibidi cell plate with a medium containing reduced phenol red. Thirty minutes before incubation with the carbonyl compounds, the cells were incubated with a 1:2000 dilution on Syto61 (Lyfe Technologies), washed with the medium and finally incubated with 150 μmol L^{-1} of compounds **1**, **3** and **4**. Throughout the experiment the cells were maintained at 37 °C in 5% CO_2. Images were obtained

by using a Zeiss LSM 710 confocal Laser Point-Scanning Microscope with a 40X oil objective lens and a numerical aperture of 1.3. COP-1 was added and excited with an argon laser with a wavelength of 488 nm, whereas Syto61 was excited using a DPSS 561-10 laser (561 nm). COP-1 was read in the green range (500-550 nm) and Syto61 in the red range (570-640 nm). The mean total fluorescence intensities of treated and untreated cells were determined with the help of ImageJ software. Statistically significant difference was tested by applying the Mann Whitney test. Data are presented in the graphs as the mean total fluorescent intensity ± SEM.

RESULTS AND DISCUSSION

Synthesis and powder characterization

The ligands dpa, bpa and pmpea were prepared by reduction of the Schiff-base formed in the condensation reaction of 2-pyridylcarboxyaldehyde and the selected primary amines.[26–28] The ligand bpea was synthesized through the reduction of the hydroxylamine formed by the reaction between 2-vinylpyridine and ammonium hydroxide.[25] The carbonyl compounds **1**–**4** were synthesized analogously to the parent compound **1**,[24] but using diethyl ether as solvent, which was used as reference to study the effect of nonbonding moiety (compound **2**) and the increase in the number of chelate members (compounds **3** and **4**) from five to six.

The carbonyl compounds synthesized showed two major CO stretching bands: a narrow band around 2025 cm^{-1} (symmetrical ν_{CO}) and a broader high intensity band around 1970-1900 cm^{-1} (double degenerate asymmetrical ν_{CO}). This indicates that all three systems deviate from the C_{3v} symmetry, either as a result of asymmetry of the first coordination sphere (compounds **2**-**4**) or to the presence of water and the formation of hydrogen bonds (compound **1**). These results are in agreement with typical CO stretching bands, which adopt a distorted facial coordination.[47,48] The spectra for compounds **1**-**4** are shown in Fig. S1-S4.

The powders of compounds **1**-**4** showed good stability in the absence of light, but compounds **2-4** showed some thermal decomposition under the experimental conditions of the elemental analysis, since these two compounds a decrease in the carbon content relative to the calculated percentage (from 43.87 to 44.47 and from 45.15 to 45.76, respectively).

Crystal structures

Compounds **1**, **3** and **4** were crystallized by slow diffusion of hexane into a dichloromethane solution at 25 °C that gave yellow crystals. Unfortunately, crystallization of **2** yielded crystals with low refractive index, which resulted in poor resolution.

The structure of **1** is similar to that published by Gonzalez and co-workers.[24] However, the crystal data obtained in this study differ, both in terms of the crystal structure and the space group, and are therefore reported herein. A striking difference between the structures is the presence of a water molecule in the lattice obtained in this study, which interacts with the uncoordinated bromide and a hydrogen atom of a methylene group, originating hydrogen bonds of 239 and 233 pm, respectively. This interaction directly influences one of the pyridine moieties, increasing the Mn1-N2 bond, when compared to the Mn1-N3 bond. Selected bond lengths of **1** are listed in Table 1 and full tables of these geometric structural parameters can be found in the Supplementary Information material. ORTEP plots of compounds **1**, **3** and **4** are shown in Fig. 2.

The structures of **3** and **4**, have some similarities with that of compound **1**. The increase in the chelate members furthers distorts the geometry, passing to a monoclinic crystal system and a C2/c space group for **3** and a triclinic crystal system and a P-1 space group for **4**. Moreover, as can be seen by the crystal structures obtained, the mild conditions employed in the synthesis procedure did not displace the bromide coordinated to the manganese center, resulting in an uncoordinated pyridine group, which can have profound effects in the CO release activity. Similar results were already reported by our group.[49] The bonds and angles are summarized in Table 1 and are compatible with values described in the literature for similar tricarbonyl compounds.[50,51]

Table 1. Selected bond lengths (Å) and angles (degrees) of **1**, **3** and **4**.

Bond lengths of compound **1** (Å)			
Mn1-C1	1.809(2)	Mn1-N1	2.0724(18)
Mn1-C2	1.803(2)	Mn1-N2	2.0624(16)
Mn1-C3	1.813(2)	Mn1-N3	2.0572(15)
Bond angles of compound **1** (degrees)			
C1-Mn1-C2	88.26(9)	C1-Mn1-N2	93.10(8)
C1-Mn1-C3	88.27(10)	C1-Mn1-N3	98.23(8)
C1-Mn1-N1	173.10(8)		
Bond lengths of compound **3** (Å)			
Mn1-C1	1.803(3)	Mn1-N1	2.101(2)
Mn1-C2	1.803(3)	Mn1-N2	2.049(2)
Mn1-C3	1.849(3)	Mn1-Br1	2.5238(4)
Bond angles of compound **3** (degrees)			
C1-Mn1-C2	88.48(13)	C1-Mn1-N2	94.50(10)
C1-Mn1-C3	90.27(11)	C1-Mn1-Br1	90.37(8)
C1-Mn1-N1	175.35(10)		
Bond lengths of compound **4** (Å)			
Mn1-C1	1.811(2)	Mn1-N1	2.1269(14)
Mn1-C2	1.8044(19)	Mn1-N14	2.11117(13)
Mn1-C3	1.8002(19)	Mn1-Br1	2.5273(3)
Bond angles of compound **4** (degrees)			
C2-Mn1-C1	85.25(9)	C2-Mn1-N14	92.58(7)
C1-Mn1-C3	90.32(8)	C2-Mn1-Br1	90.64(6)
C2-Mn1-N1	174.76(7)		

Full crystallographic tables (including structure factors) for **1**, **3** and **4** have been deposited with the Cambridge Crystallographic Data Centre under supplementary publication numbers CCDC 1824854-1824856. These data can be obtained

free of charge from the Cambridge Crystallographic Data Centre at www.ccdc.cam.ac.uk.

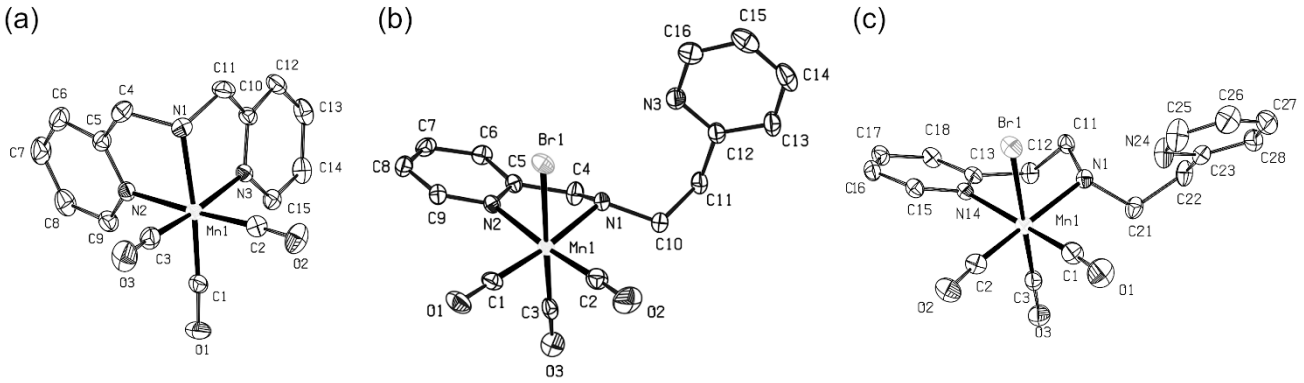

Fig. 2 ORTEP plots for the compounds with atom labeling; (a) compound **1**; (b) compound **3** and (c) compound **4**. Ellipsoids are drawn at 40% probability level. The water molecule and bromide in **1** as well as the hydrogen atoms have been omitted for clarity.

Gas-phase calculations and energy decomposition analysis

Generalized Kohn-Sham energy decomposition analysis (GKS-EDA) was conducted in order to gain insight into the effect of the first coordination sphere on the Mn-CO bonding energies and to understand why the bromide remained coordinated to the metal center under the mild conditions employed in the synthesis.

As a starting point, the crystal data were used for the geometry optimizations, resulting in structures with no imaginary frequencies. The theoretical CO stretching bands thus obtained show a good correlation with the experimental values, as can be seen in Table S1. Moreover, the theoretical results prove that compound **1**, which has a higher symmetry, adopts a κ^3 binding mode and has only two CO stretching frequencies, whereas the remainder have three CO stretching frequencies, reinforcing the κ^2 binding mode of these compounds.

The calculated interaction energies (ΔE_{int}) obtained from the EDA analysis are directly related to the dissociation energy of the carbonyls, which reflects how the ligand framework stabilizes the M-C bonds. Compound **1** shows a high degree of symmetry and all three M-CO bonds have interaction energies of -44.77, -43,98 and -43,95 kcal mol^{-1}, respectively, which shows that both the secondary amine and the pyridines contribute equally to the stabilization of the carbonyl ligands.

The substitution of a pyridine moiety by a bromide in the first coordination sphere increases the interaction energy for the M-CO bonds trans to the pyridine and the amine moieties by 2 and 4 kcal mol^{-1} respectively. However, this increase in the interaction energies is more than compensated by the decrease of the M-CO bond energy trans to the bromide unity, which shows a decrease of approximately 7 kcal mol^{-1} (around -52 kcal mol^{-1}).

This steep decrease in energy is consistent with the use of σ donating ligands in this type of compound. Overall, these values verify that ligands with a donating character, such as the bromide, promote stabilization of the M-CO bond. This is one of the reasons why mild reaction conditions do not favor the displacement of the bromide and further coordination of the pyridine moieties.

Determination of the active species in solution

Because of the elusive coordination mode of **3** and **4**, where the pyridine moiety in nonbonded, the determination of the active species in solution is essential to gain an insight into the stability of these photoCORMs. In this regard, the changes in the metal to ligand charge transfer (MLCT) at ≈350–400 nm region can reflect the changes in the first coordination sphere of the compounds.

For this reason, the changes in the UV spectra of **1**-**4** were monitored for 12 h in the dark in a noncoordinating solvent (dichloromethane) and in a coordinating solvent (acetonitrile) solvent, water was not used because of the lower solubility of the neutral compounds **2-4** in this media and the high concentrations needed to attain good quality spectra. The spectrum of compound 1 remains unchanged for both solvents during the analysis (Fig. 3a) with MLCT bands at 354 and 350 nm for dichloromethane and acetonitrile respectively, which indicates that **1** does not undergo any configurational change and has good stability in both media during the analysis.

In dichloromethane solution, compounds **2**-**4** did not show changes in the MLCT bands over time, so retained their initial values of 380, 379 and 379 nm, respectively. Changing the solvent to acetonitrile, a hypsochromic shift with clear isosbestic points was detected, as seen in Fig. 3b for **4**, (Fig. S5 for **2** and S6 for **3**) with displacements of the absorption bands to 363, 364 and 368 nm, for **2**-**4**, respectively. This behavior could be due either to the replacement of the bromide by acetonitrile, or to the bonding of the pyridine moieties for compounds **3**-**4**.

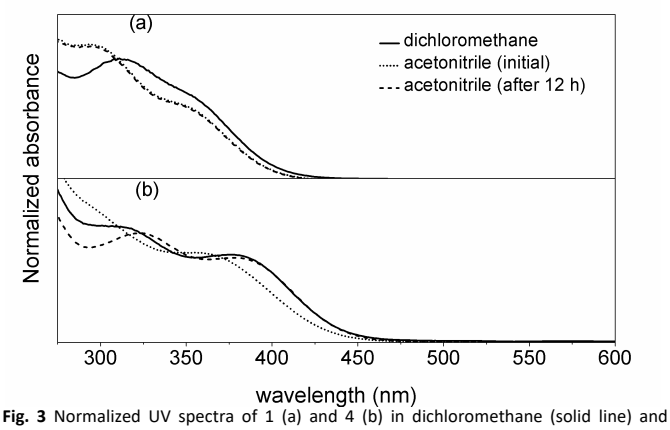

Fig. 3 Normalized UV spectra of 1 (a) and 4 (b) in dichloromethane (solid line) and acetonitrile initial (dashed line) and after 12 h incubation (dotted line).

This change in the primary coordination sphere could also be detected by IR spectroscopy, where the substitution of the bromide by a higher field ligand, in this case acetonitrile, shifts the symmetric CO stretching towards higher energy. However, as can be seen by the shifts of the IR spectra (Fig. 4a for **1**, 4b for **4**, S7 for **2** and S8 for **3**), the extent of the displacement is quite different for each compound.

In compound **2**, the changes in the symmetrical ν_{CO}, from 2025 to 2044 cm^{-1}, showed that only minor amounts of the initial compound that contains the bromide in the first coordination sphere are exchanged by acetonitrile. This hypothesis is corroborated by the absence of characteristic ESI-MS peaks, and the poor ionization of the sample (only background noise was detected). Moreover, the shift of the symmetrical ν_{CO} is compatible with the calculated values (Table S1) of the acetonitrile bound compound, as well as values reported by other groups for similar compounds.[50] For this reason, it is feasible to believe that **2** undergoes, to some extent, displacement of the bromide forming species $\mathbf{2_s}$, as shown in Fig. 5.

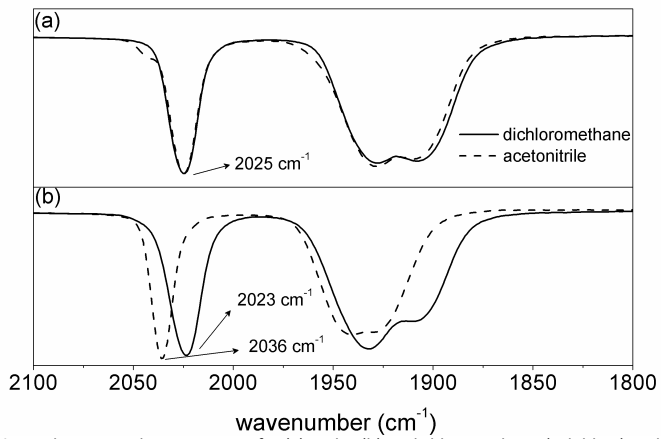

Fig. 4 Changes in the IR spectra of 1 (a) and 4 (b) in dichloromethane (solid line) and acetonitrile (dashed line) after the incubation period of 12h.

The IR spectra of **3** and **4** (Fig. S8 and 4b) display a higher degree of shift, with a displacement of the symmetrical ν_{CO}, from 2020 to 2030 and 2023 to 2036 cm^{-1} for **3** and **4**, respectively. Comparison of the symmetrical ν_{CO} shifts for **2**-**4**, make it clear that the species formed in **2** is somewhat different, because there is a 10 cm^{-1} difference. This could be due to the bonding of the nonbonded pyridine moiety, forming κ^3 compounds, forming $\mathbf{3_{py}}$-$\mathbf{4_{py}}$, as soon as $\mathbf{3_s}$-$\mathbf{4_s}$ are formed, as depicted in Fig. 5.

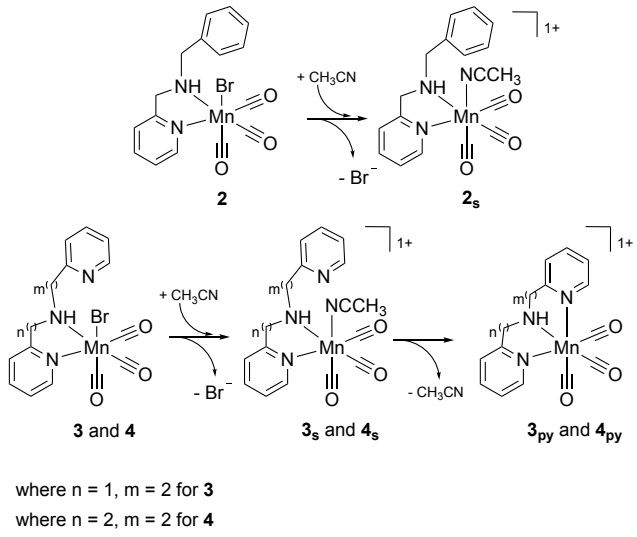

Fig. 5 Proposed species formed in solution of the photoCORMs **2**-**4**.

Moreover, although **3** showed two equal intensity peaks, **4** had a complete displacement of the band to higher energy. In addition, it is apparent from the spectra a gain in symmetry observed by the lesser degree of splitting of the degenerate stretching bands.

Another proof of this mechanism was obtained by comparing the theoretical and experimental values of the λ_{max} and ν_{CO} (Table S1), for all the possible species formed during the incubation period. These calculated values are consistent with the experimental CO stretching values obtained for $\mathbf{2_s}$ and $\mathbf{3_{py}}$-$\mathbf{4_{py}}$.

The formation of the pyridine bonded compounds was detected by ESI-MS (Fig. S9-S11), for which only one peak with a *m/z* higher than 10% intensity was detected, that is, at 352 and 366 for $\mathbf{3_{py}}$ and $\mathbf{4_{py}}$, respectively. This demonstrates that the nonbonding pyridines displace the coordinated solvent. Several attempts were made to obtain the mass spectra of $\mathbf{3_s}$-$\mathbf{4_s}$, however, these bonded acetonitrile compounds seem to have a short lifetime after the ionization process, and no fragments relative to these species were found.

These results are in agreement with the proposed mechanism of compounds like $[MnBr(CO)_3(L)]$, in which L is a bidentate ligand,[22,52] where a solvent molecule displaces the coordinated bromide in coordinating solvents. This would also explain the solubility of **2**-**4** in aqueous media, due to the formation of cationic compounds.

Specifically for $\mathbf{3_s}$-$\mathbf{4_s}$, further displacement of the solvent by the nonbonded pyridine, is also reported in the literature for compounds that adopt a κ^2 binding mode, such as $[Mn(CO)_3(tpa\text{-}\kappa^3N)]^+$ synthesized by Nagel and more recently the photoCORMs using the ligands κ^2N^1,N^2 (2,6-bis(benzimidazol-2'-yl)pyridine) and TPYOH (4'-p-*N*,*N*-bis(2-

hydroxyethyl)amino-benzyl-2,2′:6′,2″-terpyridine).[53, 54] These findings should help develop photoCORMS that can modulate the CO release process either by interaction with coordinating species that are either already part of the ligand, as in **3** and **4** or that are present in the employed media, like solvent and species present only in biological studies. Changes in the coordination sphere are seldom explored and should help modulate the CO release activity by promoting changes in CO lability as well as in the photoexcitation wavelength.

The NMR spectra of **1**, **3**, and **4** were collected at room temperature, which could provide valuable information on the binding mode and the possible displacement of the bromide by the solvent and subsequently by the pyridine moieties, could only be obtained in $CDCl_3$, limiting the information obtained. The ^{1}H NMR spectra (Fig. S12-S14) display several couplings between the hydrogen atoms mostly attributed to the conformational freedom of the nonbonding moiety, rendering the integration of the ^{1}H NMR spectra difficult and the results inconclusive.

Having knowledge of the active species in solution is essential to fine-tune the CO photorelease, because the λ_{max} and consequently the excitation wavelength are dependent on the species formed. A better insight of the influence of the species in the triggering mechanism can be understood by analyzing the orbitals associated with the MLCT band.

The major excitation attributed to the MLCT with f_{osc} above 0.01 are displayed in Fig. 6 for compound $\mathbf{3_{py}}$ and for compounds **1**-**4**, $\mathbf{2_s}$ and $\mathbf{4_{py}}$ are shown in Fig. S15. As expected, the major singlet excitations attributed to the MLCT bands, which originate from HOMO to LUMO+1 orbitals and have characteristic $\pi_{M\text{-}CO}$ to the π^*_{py} transitions.[22] Taking into consideration both the experimental and the theoretical results the changes in the first coordination sphere can modulate the excitation wavelength, and our results reinforce the concept that the σ donating character contribute to bathochromic shifts of the MLCT and thereafter of the excitation wavelength.

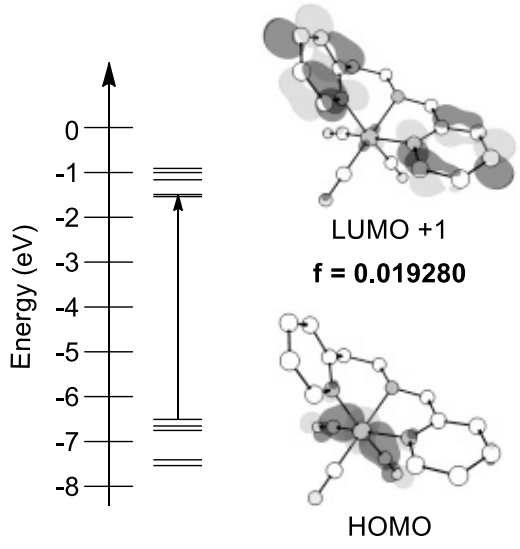

Fig. 6 Calculated frontier molecular orbital diagram of $\mathbf{3_{py}}$. The most prominent MOs involved with transitions under the lower energy band and its energy diagram are shown.

CO release studies

The CO release activity was evaluated at four wavelengths ranges: red (630 ± 10 nm), green (530 ± 5 nm), blue (460 ± 5 nm) and violet (380 ± 10 nm). Since the title compounds do not show any absorption band above 400 nm, no modification of the UV spectra was observed upon exposure to red or green light and only minor modifications were detected upon irradiation with blue light. Thereafter, the CO release activity was only evaluated by excitation in the violet region (λ_{380}), in both dichloromethane and in acetonitrile solution.

All compounds showed solvent-dependent behaviors upon exposure to λ_{380}. In dichloromethane, active species **1**-**4** maintain their coordinating sphere and there is an exponential decrease in the MLCT absorption bands, which indicates the release of CO upon light exposure and results in clear solutions. However, with acetonitrile as solvent, active species **1**, $\mathbf{2s}$, $\mathbf{3_{py}}$ and $\mathbf{4_{py}}$ show a concomitant increase in the baseline and decrease in the MLCT absorption bands, due to the formation of an oxide precipitate during the photolysis,[47,55] leading to yellow to brown solutions. Both behaviors can be seen in Fig. 7 for **4** and Fig. S16-S21 for **1**-**3**.

In both cases, the apparent CO release constants (r_{co}) and the quantum yield (Φ) were determined by monitoring the intensity of the selected wavelength over time. All data show that the active species present a linear dependence between ln[C] and time. The data for all compounds in both solvents are summarized in Table 3. As expected, in acetonitrile the CO release leads to a lower decomposition rate, both to the formation of the oxide species during photoexcitation, and the hypsochromic displacement of the MLCT in CH_3CN, either by coordination of the solvent or by the nonbonding moiety.

Therefore, the quantum yield values cannot be trusted due to the interference of the formed precipitates with the incident light and due to dispersion of the absorption values, it was calculated only for compounds **1**, **2** and **4** in the dichloromethane that presented a linear release. Furthermore, the CO release rate are coherent with the absorption bands observed for all compounds, where the fastest CO release was observed for compound **4**, which has the largest bathochromic shift, with a MLCT band closer to the λ_{380} used during the excitations.

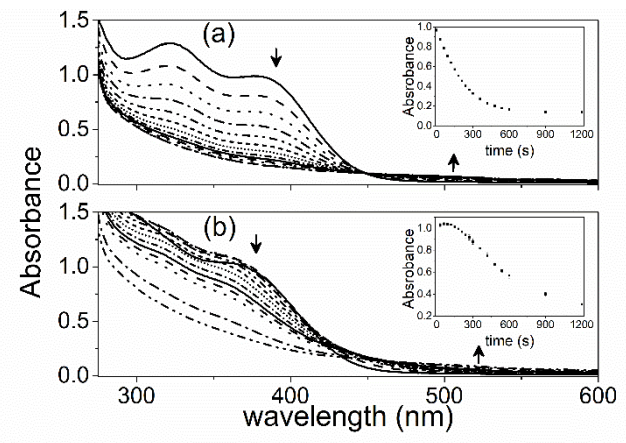

Fig. 7 (a) Changes in the UV spectrum of **4** upon light irradiation (λ_{380}) in dichloromethane; (b) Changes in the UV spectrum of $\mathbf{4_{py}}$ upon light irradiation (λ_{380}) in acetonitrile.

Table 3. Linearized constants and quantum yield for compounds **1**-**4**.

	CH_2Cl_2			CH_3CN		
	r_{co} (s^{-1}) 10^{-3}	λ_{max}	Φ	r_{co} (s^{-1}) 10^{-3}	λ_{max}	Φ
1	2.3 ± 0.1	354	0.02 ± 0.01	1.0 ± 0.1	350	-
2	4.0 ± 0.1	380	0.05 ± 0.01	3.0 ± 0.1	363	-
3	3.0 ± 0.1	379	-	1.3 ± 0.1	364	-
4	4.9 ± 0.1	379	0.06 ± 0.01	1.0 ± 0.1	368	-

The photo-released products for the irradiated samples were also analyzed by KBr IR spectra (Fig. 8 for **4** and Fig. S22-27 for **1-3**). In dichloromethane the compounds lose the CO with no defined intermediate, in acetonitrile, all compounds form a third and lower intensity band around 1870-1850 cm^{-1}, associated with the formation of a biscarbonyl intermediate.[49,53,54,56] The relative low intensity of the biscarbonyl intermediate may be due to fast oxidation of the compounds once they begin to lose the CO, as previously reported.[47,55] On comparing the relative areas after photoexcitation, all compounds lose all three CO molecules in both media.

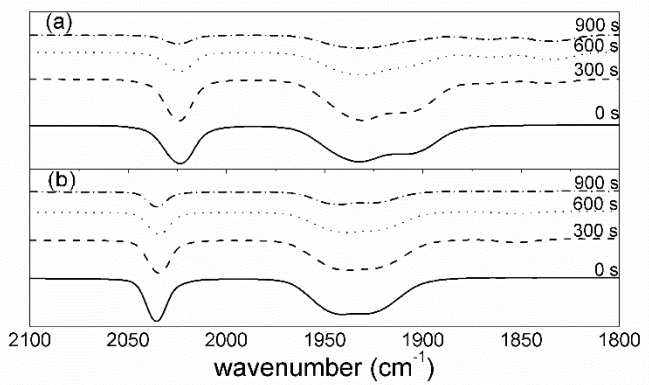

Fig. 8 (a) Changes in the IR spectrum of **4** upon light irradiation (λ_{380}) in dichloromethane; and (b) Changes in the IR spectrum of $\mathbf{4_{py}}$ upon light (λ_{380}) in acetonitrile.

CO release in aqueous solution and living cells

Having shown the potential photo-mediated CO release of compounds **1**-**4** in organic solutions, we next decide to evaluate CO release in physiological conditions, thus testing the compounds in aqueous solution and in cells. First, we determined their potential toxicity towards HeLa and HepG2 cells. Briefly, cells were incubated with a range of concentrations from 1 to 150 μmol L^{-1} of **1**-**4** for 24 h and 48 h. At these time points, a slight decrease in the percentage of live cells compared to the untreated cells was observed in the case of compounds **1**, **3** and **4**, although the percentage was always higher than 70% (Fig. 9a and S29), which indicates low toxicity of the compounds even at high concentrations (150 μmol L^{-1}). On the other hand, compound **2** promoted a strong decrease in cell viability, leading to as low as 10% of live cells after 48 h incubation, which is indicative of a higher toxicity effect.

To quantify the CO release in aqueous solution we incubated the compounds with a phosphate buffered saline solution (PBS, pH 7.4) and used the turn-on fluorescent probe COP-1 for selective CO detection, because this probe emits a green fluorescence signal in the presence of CO.[57] We observed that compounds **1**, **3** and **4** indeed release CO in aqueous solution, being compound **1** the one that exhibits a stronger release. Conversely, compound **2** strongly affects cell viability, so its CO release is only 1.6x higher than the control (Fig. 9b). This might be explained by a potential slow release of CO that may not be detected by microscopy as soon as 60 min after incubation. Moreover, CO release was higher when the complexes were irradiated with light at a wavelength of 510 nm and increased with time of exposure to COP-1, as expected (Fig. S28).

To further investigate the CO release potential of the compounds in biological conditions, HeLa cells were incubated with 150 μmol L^{-1} of compounds **1**, **3** and **4**, in the presence of COP-1. As compound **2** barely released CO in aqueous solution it was not included in these cell assays. The results show an increase in the COP-1 fluorescence in the presence of compounds **1** and **3**, in a time-dependent manner, whereas compound **4** showed no difference over time relative to the control (cells with COP-1 only), which is in agreement with the CO release observed in aqueous solution (Fig. 9c and S30). Furthermore, we observed that CO release promoted by these molecules was associated with the perinuclear region of the cells (Fig. 9c), as previously reported.[46]

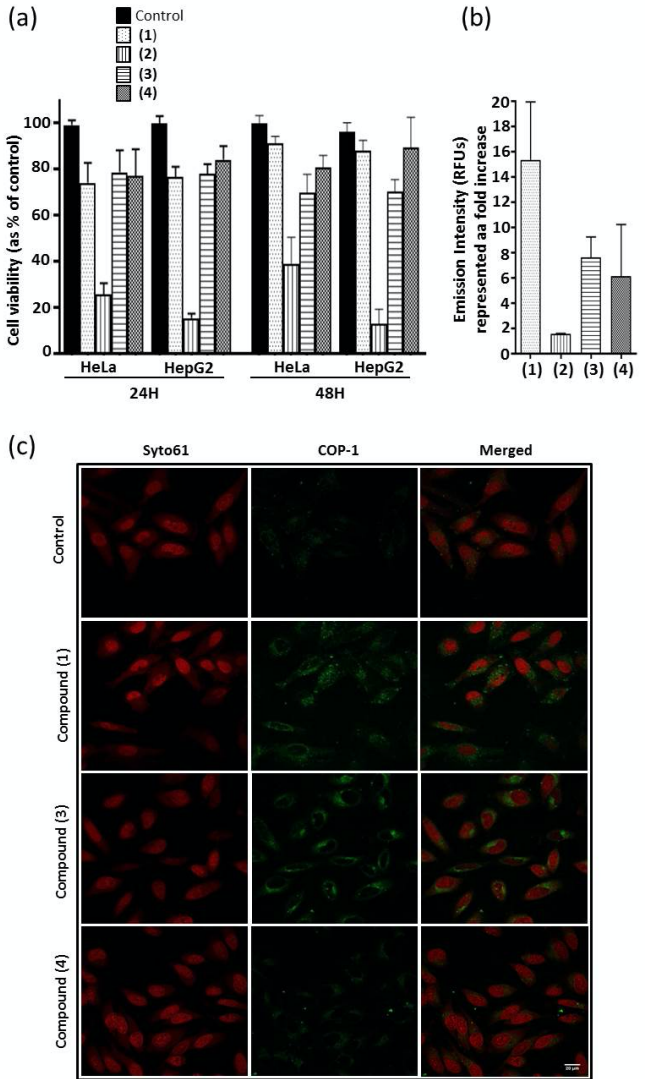

Fig. 9 CO release in aqueous solution and live cells. (a) Viability of HeLa and HepG2 cells after treatment with 150 μmol L^{-1} of compounds **1**-**4** for 24 h and 48 h. The results are shown as percentage of control (Mean + SEM of three biological replicates); (b) Histogram representing the emission intensity (RFUs – relative Fluorescent Units) measured at 60 min after incubation of 1 μM COP-1 (λ_{ex} = 475 nm) with 150 μmol L^{-1} of either **1**-**4** in PBS pH 7.4 at 37 °C. The results are shown as fold increase relative to the control (Mean + SEM of three independent experiments); (c) Representative confocal microscopy images of CO release in live HeLa cells, untreated (control) and treated with 150 μmol L^{-1} of compounds 1-4, 45 min after incubation with 1 μmol L^{-1} COP-1. Left panel – nucleic acid staining with Syto61 (red), middle panel – COP-1 turn-on response to CO (green), right panel – merged channel. Scale bar = 20 μm.

CONCLUSION

In recent years, CORMs have gained attention from several research groups that are trying to use these molecules as a CO carrier in biological systems, avoiding the drawbacks of exogenously applied CO. Trigger mechanism for the carbon monoxide release and the kinetic parameters are extensively described for several tricarbonyl compounds. In this study, three new manganese tricarbonyl compounds were synthesized and compared to the reference compound $[Mn(CO)_3(dpa)]Br$. In our synthetic approach compounds 2-4 kept a κ^2 binding mode, with a nonbonded pyridine group. This elusive binding mode was studied both in coordinating and noncoordinating solvents, which demonstrated that in coordinating solvents the bromide is replaced by a solvent molecule, which is further displaced by the nonbonded pyridine groups of **3** and **4**, proved both by IR and UV spectroscopy. Moreover, the photoactivity of compounds **1**-**4**, showed that the CO release activity was solvent dependent. In dichloromethane it was found that the linearized constants follow the trend $r_{co4} > r_{co2} > r_{co3} > r_{co1}$ and the quantum yield $\Phi_4 > \Phi_2 > \Phi_1$, which are coherent with the bathochromic shifts of the MLCT bands. Where as in acetonitrile, the compounds formed an oxide precipitate, even so the IR spectra of the photoproducts show a complete release of carbon monoxide. During the in vitro study there is a shift in the CO release activity trend, as shown by the relative fluorescent unit (RFU) values obtained. The results of this study demonstrate that even small modifications to the ligand framework, such as an increase in the chelate members, can directly influence the carbon monoxide release kinetics, both in medium.

CONFLICT OF INTEREST

The authors confirm that this article content has no conflict of interest.

ACKNOWLEDGEMENTS

The authors are grateful to the Brazilian governmental agencies CNPq (PVE – 400210/2014-2), CNPq grants were received by A. Amorim and R. A. Peralta, and INCT-Catálise. We also thank the EU Horizon 2020 programme, Marie Skłodowska-Curie ITN GA no. 675007 and TWINN-2017 ACORN, GA no. 807281, the Royal Society (UF10046 and URF\R\180019 to G. J. L. B.), FCT Portugal (iFCT IF/00624/2015 to G. J. L. B. and PhD studentship SFRH/BD/115932/2016 to A. G.) and an ERC StG (GA no. 676832) for funding, and Prof. Chris Chang for providing COP-1. This study was financed in part by the Coordenação de Aperfeiçoamento de Pessoal de Nível Superior - Brasil (CAPES) - Finance Code 001. The authors also thank CEBIME for the mass spectrometry, CAPES-PRINT, Project number 88887.310569/2018-00 and Project number 88887.310560/2018-00. The authors thank Dr Vikki Cantrill for her help with the editing of this manuscript.

SUPPLEMENTARY MATERIAL

Additional information concerning graphics and some data is provided in the supplementary information (SI) and can be obtained free of charge.

REFERENCES

1 T. A. Heinrich, R. S. da Silva, K. M. Miranda, C. H. Switzer, D. A. Wink and J. M. Fukuto, *Br. J. Pharmacol.*, 2013, **169**, 1417-1429.

2 P. Govender, S. Pai, U. Schatzschneider and G. S. Smith, *Inorg. Chem.*, 2013, **52**, 5470-5478.

3 G. Morris, B. K. Puri, A. J. Walker, M. Berk, K. Walder, C. C. Bortolasci, W. Marx, A. F. Carvalho and M. Maes, *Prog. Neuropsychopharmacol. Biol. Psychiatry*, 2019, **95**, 109708.
4 C. Peers and D. S. Steele, *J. Mol. Cell. Cardiol.*, 2012, **52**, 359-365.
5 J. J. Rose, L. Wang, Q. Xu, C. F. McTiernan, S. Shiva, J. Tejero and M. T. Gladwin, *Am. J. Respir. Crit. Care Med.*, 2017, **195**, 596-606.
6 S. Abid, A. Houssaini, N. Mouraret, E. Marcos, V. Amsellem, F. Wan, J. L. Dubois-Rande, G. Derumeaux, J. Boczkowski, R. Motterlini and S. Adnot, *Arterioscler. Thromb. Vasc. Biol.*, 2014, **34**, 304-312.
7 W. Fan, F. Huang, Z. Wu, X. Zhu, D. Li and H. He, *J. Neurosci. Res.*, 2011, **89**, 802-807.
8 W. J. Wilkinson and P. J. Kemp, *J. Physiol.*, 2011, **589**, 3055-3062.
9 S. Garcia-Gallego and G. J. L. Bernardes, *Angew. Chem. Int. Ed.*, 2014, **53**, 9712-9721.
10 M. A. Gonzales and P. K. Mascharak, *J. Inorg. Biochem.*, 2014, **133**, 127-135.
11 H. H. Kim and S. Choi, *Int. J. Mol. Sci.*, 2018, **19**.
12 M. Kourti, W. G. Jiang and J. Cai, *Oxid. Med. Cell Longev.*, 2017, **2017**, 9326454.
13 R. Motterlini and L. E. Otterbein, *Nat. Rev. Drug Discov.*, 2010, **9**, 728-743.
14 C. C. Romao, W. A. Blattler, J. D. Seixas and G. J. L. Bernardes, *Chem. Soc. Rev.*, 2012, **41**, 3571-3583.
15 R. Kretschmer, G. Gessner, H. Gorls, S. H. Heinemann and M. Westerhausen, *J. Inorg. Biochem.*, 2011, **105**, 6-9.
16 A. R. Marques, L. Kromer, D. J. Gallo, N. Penacho, S. S. Rodrigues, J. D. Seixas, G. J. L. Bernardes, P. M. Reis, S. L. Otterbein, R. A. Ruggieri, A. S. G. Gonçalves, A. M. L. Gonçalves, M. N. D. Matos, I. Bento, L. E. Otterbein, W. A. Blättler and C. C. Romão, *Organometallics*, 2012, **31**, 5810-5822.
17 U. Schatzschneider, *Inorganica Chim. Acta*, 2011, **374**, 19-23.
18 F. Zobi, O. Blacque, R. A. Jacobs, M. C. Schaub and A. Y. Bogdanova, *Dalton Trans.*, 2012, **41**, 370-378.
19 G. P. Pfeifer, Y. H. You and A. Besaratinia, *Mutat. Res.*, 2005, **571**, 19-31.
20 N. E. Brückmann, M. Wahl, G. J. Reiß, M. Kohns, W. Wätjen and P. C. Kunz, *Eur. J. Inorg. Chem.*, 2011, **2011**, 4571-4577.
21 M. P. Coogan and J. A. Platts, *Chem. Commun.*, 2016, **52**, 12498-12501.
22 I. Chakraborty, S. J. Carrington and P. K. Mascharak, *Acc. Chem. Res.*, 2014, **47**, 2603-2611.
23 J. Jimenez, I. Chakraborty and P. K. Mascharak, *Eur. J. Inorg. Chem.*, 2015, **2015**, 5021-5026.
24 M. A. Gonzalez, M. A. Yim, S. Cheng, A. Moyes, A. J. Hobbs and P. K. Mascharak, *Inorg. Chem.*, 2012, **51**, 601-608.
25 S. A. Leaver, M. Palaniandavar, C. A. Kilner and M. A. Halcrow, *Dalton Trans.*, 2003, 4224-4225.
26 A. Neves, M. A. de Brito, I. Vencato, V. Drago, K. Griesar and W. Haase, *Inorg. Chem.*, 1996, **35**, 2360-2368.
27 C. Piovezan, J. M. Silva, A. Neves, A. J. Bortoluzzi, W. Haase, Z. Tomkowicz, E. E. Castellano, T. C. Hough and L. M. Rossi, *Inorg. Chem.*, 2012, **51**, 6104-6115.
28 Y.-w. Ren, A.-z. Wu, H.-y. Liu and H.-f. Jiang, *Transit. Met. Chem.*, 2010, **35**, 191-195.
29 APEX2, SAINT and SADABS software, version 2011.8-0, Bruker AXS Inc., Madison, Wisconsin, USA.
30 G. Sheldrick, *Acta Crystallogr. C*, 2015, **71**, 3-8.
31 A. Spek, *Acta Crystallogr. D*, 2009, **65**, 148-155.
32 P. Hohenberg and W. Kohn, *Phys. Rev.*, 1964, **136**, B864 - B871.
33 W. Kohn and L. J. Sham, *Phys. Rev.*, 1965, **140**, A1133-A1138.
34 J. P. Perdew, *Phys. Rev. B Condens. Matter.*, 1986, **33**, 8822-8824.
35 S. Grimme, J. Antony, S. Ehrlich and H. Krieg, *J. Chem. Phys.*, 2010, **132**, 154104.
36 K. Eichkorn, F. Weigend, O. Treutler and R. Ahlrichs, *Theor. Chem. Acc.*, 1997, **97**, 119-124.
37 A. Schäfer, H. Horn and R. Ahlrichs, *J. Chem. Phys.*, 1992, **97**, 2571-2577.
38 A. Schäfer, C. Huber and R. Ahlrichs, *J. Chem. Phys.*, 1994, **100**, 5829-5835.
39 F. Neese, *WIREs Comput. Mol. Sci.*, 2012, **2**, 73-78.
40 M. W. Schmidt, K. K. Baldridge, J. A. Boatz, S. T. Elbert, M. S. Gordon, J. H. Jensen, S. Koseki, N. Matsunaga, K. A. Nguyen, S. Su, T. L. Windus, M. Dupuis and J. A. Montgomery Jr, *J. Comput. Chem.*, 1993, **14**, 1347-1363.
41 S. F. Boys and F. Bernardi, *Mol. Phys.*, 2002, **100**, 65-73.
42 E. Runge and E. K. U. Gross, *Phys. Rev. Lett.*, 1984, **52**, 997-1000.
43 A. D. Becke, *J. Chem. Phys.*, 1993, **98**, 5648-5652.
44 P. J. Stephens, F. J. Devlin, C. F. Chabalowski and M. J. Frisch, *J. Phys. Chem.*, 1994, **98**, 11623-11627.
45 A. V. Marenich, C. J. Cramer and D. G. Truhlar, *J. Phys. Chem. B*, 2009, **113**, 6378-6396.
46 B. W. Michel, A. R. Lippert and C. J. Chang, *J. Am. Chem. Soc*,. 2012, **134**, 15668-15671.
47 H.-M. Berends and P. Kurz, *Inorganica Chim. Acta*, 2012, **380**, 141-147.
48 W. Huber, R. Linder, J. Niesel, U. Schatzschneider, B. Spingler and P. C. Kunz, *Eur. J. Inorg. Chem.*, 2012, **2012**, 3140-3146.
49 A. L. Amorim, M. M. Peterle, A. Guerreiro, D. F. Coimbra, R. S. Heying, G. F. Caramori, A. L. Braga, A. J. Bortoluzzi, A. Neves, G. J. L. Bernardes and R. A. Peralta, *Dalton Trans.*, 2019, **48**, 5574-5584.
50 M. A. Gonzalez, S. J. Carrington, N. L. Fry, J. L. Martinez and P. K. Mascharak, *Inorg. Chem.*, 2012, **51**, 11930-11940.
51 F. Mohr, J. Niesel, U. Schatzschneider and C. W. Lehmann, *Z. Anorg. Allg. Chem.*, 2012, **638**, 543-546.
52 T. N. Twala, M. Schutte-Smith, A. Roodt and H. G. Visser, *Dalton Trans.*, 2015, **44**, 3278-3288.
53 A. M. Mansour and A. Friedrich, *Inorg. Chem. Front.*, 2017, **4**, 1517-1524.
54 C. Nagel, S. McLean, R. K. Poole, H. Braunschweig, T. Kramer and U. Schatzschneider, *Dalton Trans.*, 2014, **43**, 9986-9997.
55 U. Sachs, G. Schaper, D. Winkler, D. Kratzert and P. Kurz, *Dalton Trans.*, 2016, **45**, 17464-17473.
56 Q. Jiang, Y. Xia, J. Barrett, A. Mikhailovsky, G. Wu, D. Wang, P. Shi and P. C. Ford, *Inorg. Chem.*, 2019, **58**, 11066-11075.
57 S. McLean, B. E. Mann and R. K. Poole, *Anal. Biochem.*, 2012, **427**, 36-40.

